Journal of Composites Science

MDPI

Article

Investigation of the Cyclic Behavior of Unidirectional rCFRP with Focus on the Characterization of the Residual Strength Behavior

Philipp Reiser *, Christian Becker , Andreas Baumann, Nicole Motsch-Eichmann and Joachim Hausmann *

Leibniz-Institut für Verbundwerkstoffe GmbH, 67663 Kaiserslautern, Germany;
christian.becker@leibniz-ivw.de (C.B.); andreas.baumann@leibniz-ivw.de (A.B.);
nicole.motsch@leibniz-ivw.de (N.M.-E.)

* Correspondence: philipp.reiser@leibniz-ivw.de (P.R.); joachim.hausmann@leibniz-ivw.de (J.H.);
Tel.: +49-631-2017-415 (P.R.); +49-631-2017-301 (J.H.)

Abstract

This paper investigates the fatigue and residual strength behavior of recycled carbon fiber reinforced plastics (rCFRPs) with different fiber architectures in an epoxy resin matrix: a unidirectional (UD) rCFRP and a non-crimp fabric (NCF) composite. Due to the research gap in fatigue testing of recycled carbon fiber-reinforced plastics with quasi-continuous fiber reinforcement, their fatigue properties are investigated in this article. The objective of the present study is to contribute to the broader goal of integrating recycled carbon fibers as quasi-continuous fiber reinforcement in structural applications by understanding their failure behavior. To determine suitable stress levels for fatigue testing, quasi-static tensile tests are conducted first. Subsequently, fatigue tests are performed with a stress ratio of 0.1. Damage evolution is documented by a continuous recording of the stiffness degradation. For the unidirectional material, an S-N_f curve is created based on three stress levels. The curve can be described with a logarithmic equation. Fatigue testing of the NCF laminate is performed at a single stress level. Subsequent residual strength tests using standard specimens show no clear correlation between the number of load cycles of pre-cycling and residual strength, but indicate a sudden-death behavior for both composites. For further investigation of the damage behavior, in situ residual strength tests are carried out using a combination of acoustic emission analysis and micro-computed tomography (μCT) imaging. This investigation is intended to illustrate crack initiation and propagation three-dimensionally after pre-cycling and during residual strength tests. The results demonstrate a significant influence of the microstructure on the failure behavior.

Keywords: recycled carbon fibers (rCFs); staple fiber yarn; epoxy resin matrix; unidirectional rCFRP; non-crimp fabric composite; fatigue testing of rCFRP; non-destructive testing; acoustic emission analysis; in situ micro-computed tomography (μCT)

Check for updates

Academic Editor: Nithya Subramanian

Received: 26 January 2026
Revised: 27 February 2026
Accepted: 5 March 2026
Published: 7 March 2026

1. Introduction

Lightweight materials such as fiber-reinforced plastics are essential in industrially important sectors (e.g., transportation) [1,2]. Among these, carbon fiber-reinforced plastics play a key role due to their specific mechanical properties. However, the energy-intensive production of carbon fibers in particular makes the development of an efficient circular economy essential [3,4]. Fiber–matrix separation offers the possibility to recover recycled carbon fibers (rCFs) from production residues or end-of-life components. These recycled fibers can be further processed into staple fiber yarns (spun long fibers), which allows the production of components with a quasi-continuous fiber reinforcement. Compared to a statistically distributed fiber orientation, e.g., in chopped strand mats, staple fiber yarns made from recycled fibers offer the possibility of aligned fiber placement. This is intended to allow the fibers to be placed specifically in the load direction. Furthermore, rCF staple fiber yarns can be further processed into semi-finished products such as non-crimp fabrics, enabling bidirectional fiber reinforcement with good handling properties without undulations (as in woven fabrics) reducing the mechanical properties [5].

This paper investigates two types of recycled carbon fiber-reinforced plastics (rCFRPs): a unidirectional rCFRP and a non-crimp fabric composite. Both are made from recycled staple fiber yarns and an epoxy resin matrix. Understanding the mechanical properties of these materials is essential for component design. While their quasi-static tensile properties have already been analyzed in other studies [6,7], the fatigue properties have not yet been investigated. Many structural components are subjected to cyclic loading during operation, so fatigue properties are also important and must therefore be investigated. This is the first time that this has been done for the materials under investigation in this study [8].

In non-recycled continuous fiber composites, fatigue in unidirectional laminates typically starts with matrix crack initiation, preferably at defects (e.g., pores or fiber defects). This is followed by matrix crack propagation perpendicular to the load direction, leading to fiber–matrix debonding or the formation of fiber-bridged matrix cracks depending on the fiber–matrix adhesion and the local fiber orientations. If sufficiently advanced, this leads to fatigue failure [9–11].

In non-crimp fabric laminates (e.g., $[0/90]_s$), fatigue is initially characterized by the formation of cracks in the 90° layers, which propagate to the adjacent 0° layers. This is followed by delamination or fiber fractures in the 0° layers, ultimately leading to failure [9–12].

The objective of this study is to conduct the first investigation of fatigue properties of recycled carbon fiber-reinforced plastics with quasi-continuous fiber reinforcement, manufactured from rCF staple fiber yarns. Additionally, the aim is to answer the question of how the fatigue behavior of rCFRP materials differs from that of non-recycled continuous fiber materials. The findings aim to support the broader goal of integrating recycled carbon fiber yarns in structural applications by understanding their failure behavior. For this purpose, fatigue tests and residual strength tests on standard specimens are conducted. To get a better understanding of the micromechanical processes within the rCFRP materials, micro-computed tomography examinations are also performed during an in situ residual strength test with tapered specimens. This should provide detailed information about crack initiation and propagation behavior in the materials investigated. In addition, the in situ tests are combined with an acoustic emission analysis.

2. Materials and Methods

2.1. Description of the Manufactured Materials

The materials investigated consist of recycled carbon fibers from carbon fiber scrap (e.g., spool ends) embedded in an epoxy resin matrix. Two fiber architectures are studied: a unidirectional architecture made from staple fiber yarn and a non-crimp fabric layup. The NCF laminate also consists of staple fiber yarns and has a symmetric stacking sequence of $[0/90/90/0]_s$.

The staple fiber yarn used (Wagenfelder Spinnereien GmbH, Wagenfeld, Germany) for the unidirectional material consists of 90 wt% recycled carbon fibers fixed by a polyamide 6 yarn wound around the rCF (Figure 1a). Additionally, it also contains polyamide 6 staple fibers aligned parallel to the rCF to adjust the desired rCF fiber content. The polyamide

6 content is 10 wt%. The non-crimp fabric (Figure 1b) consists of 80 wt% rCF and 20 wt% polyamide 6 fibers [13].

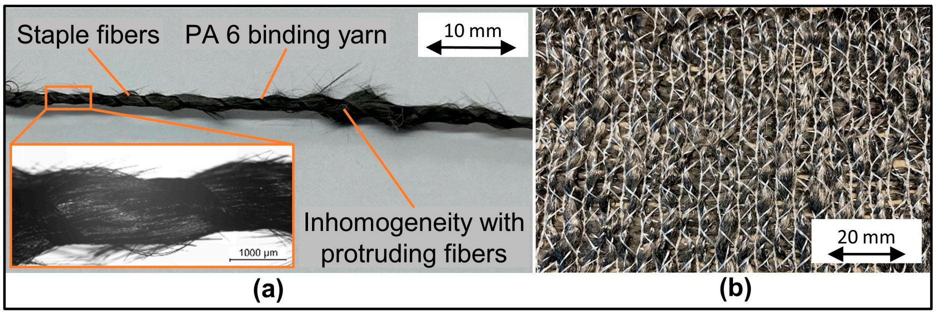

Figure 1. (**a**) rCF staple fiber yarn, (**b**) non-crimp fabric [0/90].

The unidirectional material was produced using a wet winding process, with four layers of roving applied sequentially. The non-crimp fabric composite was produced using a hand lay-up method with 4 layers of the NCF, where 1 layer consists of 0° and 90° fibers [0/90] fixed by a polymer yarn. Both materials used an epoxy resin matrix (Huntsman epoxy resin Araldite LY 1135-1, hardener Aradur 917 and Accelerator 960-1 in a mass ratio of 100:90:2, Huntsman Corporation, The Woodlands, TX, USA). The laminates were consolidated and cured in an autoclave under pressure between metal cover plates. The maximum curing temperature of 140 °C was applied for 6 h. The rCF volume fractions (Table 1) were calculated based on the masses of carbon fibers and polymers introduced. Therefore, the staple fiber yarn was weighed to determine the masses of recycled carbon fibers and PA 6 fibers. After consolidation and curing, the plate was weighed to quantify the epoxy resin content.

Table 1. rCFRP materials and investigations.

Plate	Mean Plate Thickness in mm	rCF Volume Fraction in %	Investigation
UD1	2.50	35	Quasi-static tensile test, fatigue test, residual strength test
UD2	2.12	40	Quasi-static tensile test, in situ residual strength test
G1	2.22	37.5	Quasi-static tensile test
G2	2.06	39.5	Fatigue test
G3	2.18	40.5	Residual strength test
G4	2.06	40	Residual strength test, in situ residual strength test
G5	2.23	37.5	In situ residual strength test

The fiber volume fractions (FVFs) can be found in Table 1, which also shows which laminates were used for the investigations that follow. As a result of the inhomogeneity of the fiber materials used (Figures 1 and 2) and the varying plate thicknesses (Table 1), different fiber volume fractions were observed in the differently manufactured sheets of the same material. Due to the pronounced differences in the fiber volume fractions of the two unidirectional materials, the fatigue and residual strength tests with standard specimens were conducted with material UD1, while UD2 was used for the in situ residual strength tests. For the non-crimp fabric composites (G), the laminates tested are considered mechanically equivalent due to the pronounced inhomogeneities of the rCF non-crimp fabric, even within one laminate (Figure 2b).

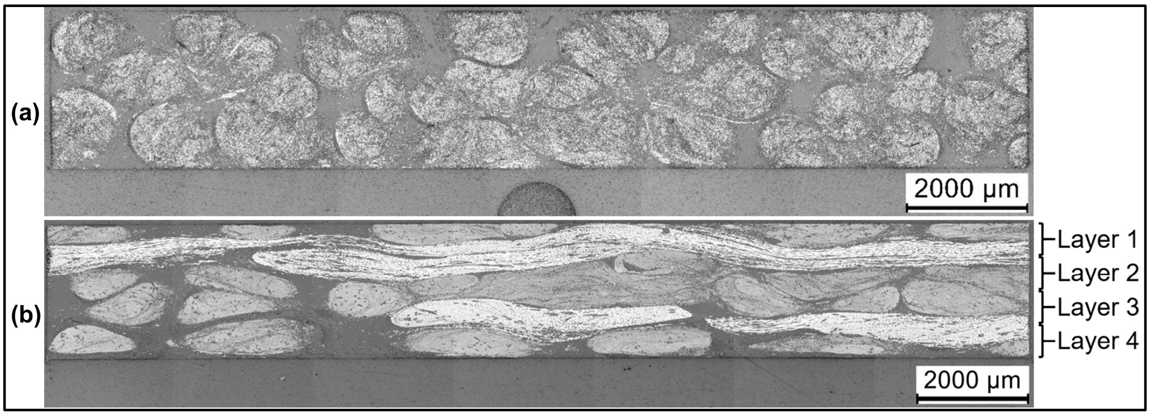

Figure 2. Micrographs of the manufactured sheet materials: (**a**) Unidirectional material UD1, (**b**) non-crimp fabric composite G1 (view in 0° direction).

Figure 2 shows micrographs of the produced materials. There is no pronounced porosity evident. However, inhomogeneities in the rCFRP materials are noticeable, such as resin- and fiber-rich areas and fiber disorientation, due to the structure of the fiber materials and the manufacturing processes. This leads to locally different fiber volume fractions. Fiber orientation is further influenced by the yarn undulation (Figure 1a).

2.2. Description of the Mechanical Investigations of Standard Specimens

To determine suitable stress levels for the fatigue tests, quasi-static tensile tests were first conducted to determine the ultimate tensile strength at static loading rate (UTS^s). These tests were performed in accordance with EN ISO 527-5 [14] and DIN EN ISO 527-1 [15]. The specimen geometry was 250 mm × 25 mm. Five specimens per material were examined. The tests were performed at a speed of 2 mm/min. Force was measured using a 100 kN load cell. An optical measuring system (ARAMIS v6.3.0 digital image correlation system) was used to evaluate the specimen strain. Images were recorded at 5 frames per second.

Load-controlled fatigue tests were based on ISO 13003 [16] and carried out with a stress ratio of 0.1 and a test frequency of 5 Hz. The specimen geometry was 250 mm × 15 mm. Force was measured using a 40 kN load cell. The tests were carried out at room temperature. For the unidirectional material, three stress levels (80%, 70% and 60% of the UTS^s) were defined, which served as maximum stresses for the fatigue tests. A lifetime diagram (S/UTS^s-N_f-curve) was then created. Due to material limitations, the non-crimp fabric laminate was tested only at 50% of the UTS^s as the maximum cyclic stress. Nevertheless, the failure behavior and the residual strength could still be investigated and compared to those of the unidirectional material, providing insights into differences in fatigue damage evolution and mechanical properties.

The S/UTS^s-N_f-diagrams (Figure 6) were evaluated using a procedure based on DIN 50100 (Chapter 10.2.3 of [17]). The following Equations (1)–(4) are taken from Ref. [17]. A log-normal distribution of the number of cycles to failure was assumed. The evaluation was carried out at each stress level, starting with the calculation of the mean logarithmic number of cycles to failure $N_{50\%}$ (50% survival probability, Figure 6), according to Equation (1). For each level, the number of cycles to failure for survival probabilities of 90% and 10% were determined and marked in the diagram (Figure 6), according to Equations (3) and (4).

Ref. [17] states that the standard deviation for small sample sizes (less than 10) must be adjusted using a correction factor (Equation (2)).

$$N_{50\%} = 10^{\frac{1}{n}\sum_{i=1}^{n}\log(N_i)} \tag{1}$$

$$s_c = \frac{n-0.74}{n-1} \cdot \sqrt{\frac{1}{n-1}\sum_{i=1}^{n}\left(\log(N_i) - \log(N_{50\%})\right)^2} \tag{2}$$

$$N_{90\%} = 10^{\log(N_{50\%})-1.282\cdot s_c} \tag{3}$$

$$N_{10\%} = 10^{\log(N_{50\%})+1.282\cdot s_c} \tag{4}$$

The stiffness degradation evaluation was performed using the crosshead displacement of the servo-hydraulic testing machine during load-controlled fatigue testing. Peak-valley data from the machine was used to determine changes in dynamic stiffness.

$$E_{dyn} = \frac{\sigma_{peak} - \sigma_{valley}}{\varepsilon_{peak} - \varepsilon_{valley}} = \frac{\frac{F_{peak}-F_{valley}}{A}}{\frac{x_{peak}-x_{valley}}{L_0}} \tag{5}$$

Equation (5) shows the calculation of dynamic stiffness based on the peak-valley data. This includes the force (F) and the displacement (x) data at the maximum (peak) and minimum (valley) force at each cycle of the fatigue test. A denotes the unloaded sample cross-sectional area, and L_0 denotes the clamping length between the clamping jaws of the machine.

Residual strength tests are intended to show how the residual load-bearing capacity of the materials changes based on different degrees of pre-damage introduced by preceding cyclic loading. The test parameters corresponded to those mentioned above. The selected stress levels for pre-cycling were 70% of the UTS^s for the unidirectional material and 50% of the UTS^s for the non-crimp fabric composite. To avoid unintentional failure of the specimens intended for the residual strength testing, specimens were subjected to 25%, 50% and 75% of the lowest number of cycles to failure at each stress level of the previously conducted fatigue tests (Figure 6). This means that pre-cycling of the unidirectional specimens was performed with 1575, 3150 and 4725 load cycles, and for the non-crimp fabric laminate with 1225, 2450 and 3675 cycles. This choice focused on the low-cycle fatigue regime.

2.3. Description of the In Situ Residual Strength Tests of Tapered Specimens

Following the residual strength tests on standard specimens, in situ residual strength tests were performed in an X-ray microscope. This enabled the observation of microstructural material behavior after fatigue loading and during the residual strength tests.

An in situ testing device (Deben CT5000, Deben UK Ltd., Woolpit, Suffolk, UK, Figure 3d) was used to perform in situ residual strength tests within the micro-computed tomography (Carl Zeiss Xradia 520, Carl Zeiss AG, Oberkochen, Germany, Figure 3e). For this purpose, tensile specimens similar to the standard specimens, but with a width of 22 mm, were pre-cycled as described in Section 2.2. These specimens were then milled into a tapered geometry for in situ residual strength testing (Figure 3a). Pre-cycling was carried out on standard specimens before milling to ensure that any damage introduced by the milling cutter had no effect during cyclic loading. The standard specimens were cut using a universal wet-abrasive cut-off machine, which ensured a better quality of the specimen edges compared to milling. For the in situ residual strength testing, the specimen edges must be considered separately in the µCT inspection, as additional damage could be introduced during milling. These tests were conducted with a test speed of 1 mm/min, with force measured using the built-in 5 kN load cell.

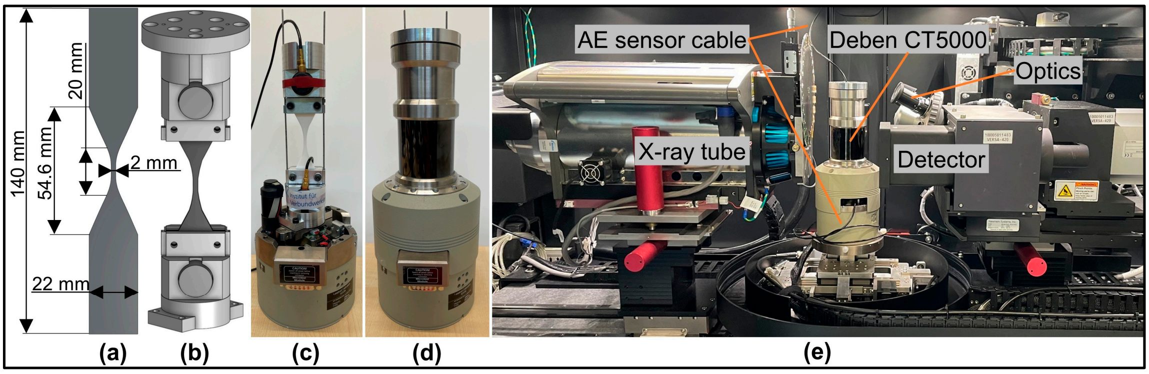

Figure 3. (**a**) Specimen geometry for in situ testing (narrowest width: 2 mm for unidirectional material, 2.8 mm for non-crimp fabric composite), (**b**) clamping device for in situ test device with acoustic emission sensors, (**c**,**d**) in situ test device Deben CT5000, (**e**) Deben CT5000 in Carl Zeiss Xradia 520 X-ray microscope.

The in situ system was equipped with acoustic emission sensors (Vallen VS150-M [18], Vallen Systeme GmbH, Wolfratshausen, Germany, see Figure 3c) integrated into the gripping device of the system to record acoustic events in the material while testing. Pre-amplification was 34 dB (Vallen AEP4 [19]). The detection threshold for the acoustic activity recording was set to 43 dB.

The recorded AE-signals provide information about the onset and progression of damage within the specimen. Using the acoustic emissions, the strain levels at which the tensile test was interrupted (displacement kept constant) were determined, and a micro-computed tomography scan was performed. After each scan, testing continued. The interruptions were performed when the following load levels were reached:

- Load Level LL0: Pre-cycled condition, before quasi-static loading
- Load Level LL1: Onset of acoustic emissions during the in situ residual strength test
- Load Level LL2: After a significant accumulation of acoustic emissions
- Load Level LL3: After failure occurs in the in situ residual strength test

For the non-crimp fabric composite, all of the previously mentioned load levels were examined. For the unidirectional material, the examinations were limited to load levels LL0 and LL1, as the in situ facility, with its maximum testing force of 5 kN, could not completely cause the unidirectional specimens to fail.

3. Results

3.1. Quasi-Static Tensile Tests

Both materials tested, the unidirectional material and the non-crimp fabric composite, exhibit a quasi-linear relationship between stress and strain in the quasi-static tensile tests until failure (Figure 4). The stress–strain data were smoothed using a Savitzky–Golay filter (window size of 11 and polynomial order of 1) to reduce noise while preserving the curve shape.

The average tensile properties are shown in Table 2.

The tensile strengths UTS^s of UD1 (871 MPa) and G1 (403 MPa) are of particular interest for defining the stress levels used in the following fatigue tests.

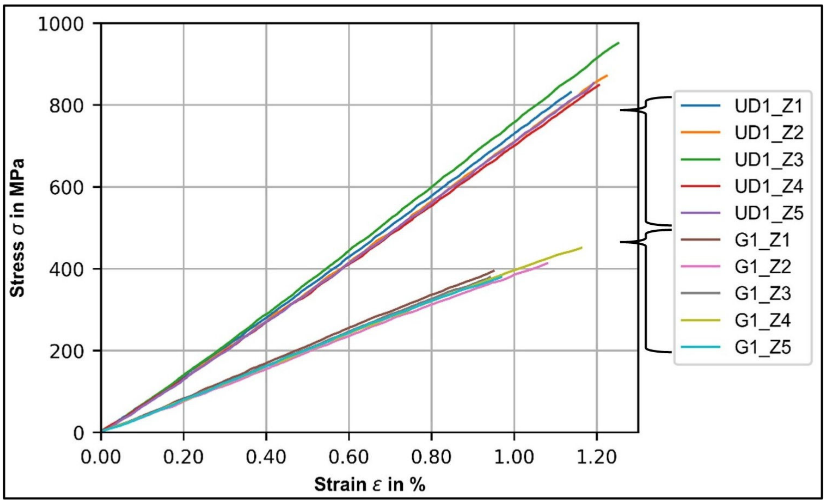

Figure 4. Stress–strain diagram from the quasi-static tensile tests of the unidirectional material UD1 and the non-crimp fabric composite G1 (for clarity, the graphs of material UD2 are not shown).

Table 2. Quasi-static tensile properties (mean values and standard deviations s).

Plate	E in MPa	ε_m in %	UTS^s in MPa
UD1	68,834 ($s_{E,UD1}$ = 1800)	1.20 ($s_{\varepsilon,UD1}$ = 0.04)	871 ($s_{UTS,UD1}$ = 47)
UD2	71,940 ($s_{E,UD2}$ = 2453)	1.09 ($s_{\varepsilon,UD2}$ = 0.04)	846 ($s_{UTS,UD2}$ = 45)
G1	40,374 ($s_{E,G1}$ = 2457)	1.02 ($s_{\varepsilon,G1}$ = 0.10)	403 ($s_{UTS,\,G1}$ = 31)

When considering the failure behavior of the materials, it can be seen that the unidirectional material exhibits pronounced crack formation in the longitudinal direction of the specimen (Figure 5a), while the non-crimp fabric composite tends to form one or more cracks approximately perpendicular to the load direction (Figure 5b). It is known from SEM fracture surface observations in [6,7] that fiber pullouts and inter-fiber fractures (longitudinal cracking as shown in Figure 5a) dominate as failure mechanisms for the unidirectional material due to the poor fiber–matrix adhesion. Observations of the damage mechanisms are made in Section 3.4, where the results of in situ residual strength investigations are considered.

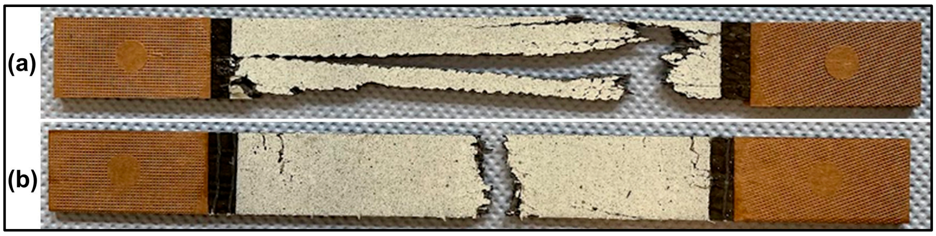

Figure 5. Fractured specimens from the quasi-static tensile tests: (**a**) Unidirectional material, (**b**) non-crimp fabric composite.

3.2. Fatigue Testing

To evaluate the fatigue tests, normalized S/UTS^s-N_f diagrams (Figure 6) and stiffness degradations (Figure 7) are considered. For the S/UTS^s-N_f diagrams, the applied normalized stress level S/UTS^s is plotted against the number of cycles to failure N_f. S/UTS^s is used to describe a stress level that relates the maximum stress of fatigue loading S to the tensile strength UTS^s of the material. For stiffness degradation, the relative dynamic stiffness $E_{dyn}/E_{dyn,1}$ is plotted over the relative fatigue life N/N_f, where $E_{dyn,1}$ is the dynamic stiffness during the first load cycle.

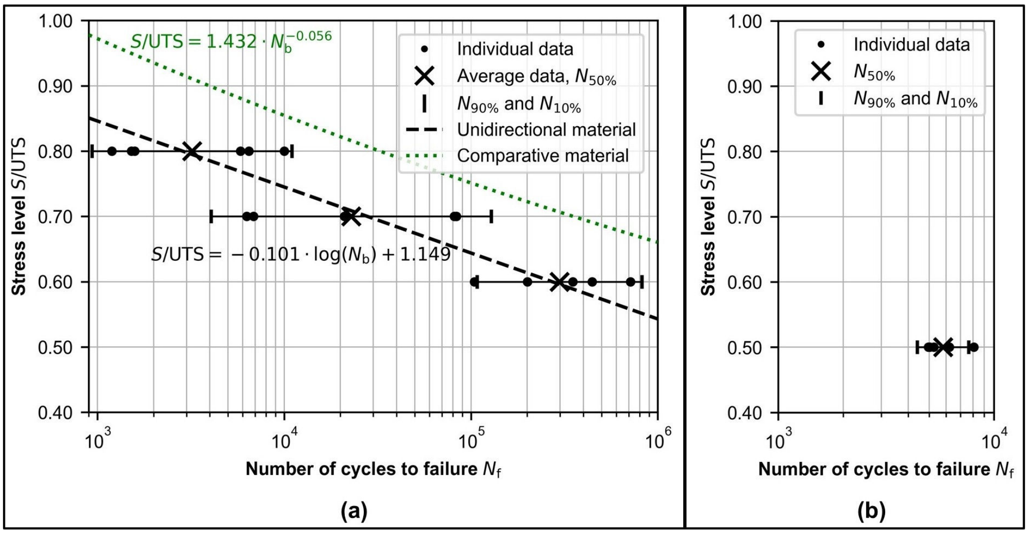

Figure 6. S/UTS^s-N_f diagrams of the fatigue tests: (**a**) Unidirectional rCFRP and comparative material [20], (**b**) non-crimp fabric composite.

The S/UTS^s-N_f diagrams resulting from the fatigue tests are shown in Figure 6. The figure shows the number of cycles to failure for the individual specimens tested as dots. For the unidirectional material, there is a pronounced FRP-typical scatter of the number of cycles to failure of approximately one order of magnitude (Figure 6a) [9].

Based on the average data (Figure 6a), a regression line for the unidirectional material can be described with a logarithmic equation:

$$S/\mathrm{MPa} = 1000.78 - 87.97 \cdot \log(N_f) \quad (6)$$

It is not possible to make any reliable statements about the fatigue behavior of the material outside the investigated range of Figure 6a. Furthermore, no fatigue limit was determined.

For comparison, Figure 6a also shows a normalized S/UTS^s-N_f curve of a unidirectional continuous non-recycled carbon fiber composite (Figure 6a, green). These data are based on [20] and refer to a material (vCFRP) with a fiber volume fraction of 30%. The vCFRP material was produced using a vacuum assisted resin transfer molding process with a bindered carbon-fiber preform (Angeloni Group S.r.l. HS 15-50) and an epoxy resin matrix (Huntsman EPIKOTE Resin MGS RIMR135 with EPIKOTE Curing Agent MGS RIMH1366). The tensile strength parallel to the fiber direction is approximately 1025 MPa [20].

Measurement data for failure load cycles in the range of approximately 10^3 and 10^6 are available for both materials: rCFRP and vCFRP (Figure 6a). While the slopes of the curves are comparable, the reference material's curve is shifted to approximately 10% larger S/UTS^s ratios, indicating a better fatigue resistance [20].

For the non-crimp fabric composite, the number of cycles to failure at the stress level investigated is shown in Figure 6b.

The macroscopic failure behavior observed in the fatigue tests occurs during the last load cycle as sudden failure with similar characteristics as in the quasi-static tensile tests (Figure 5). Section 3.4 is dedicated to the detailed description of the microstructural damage during fatigue and residual strength tests for both materials.

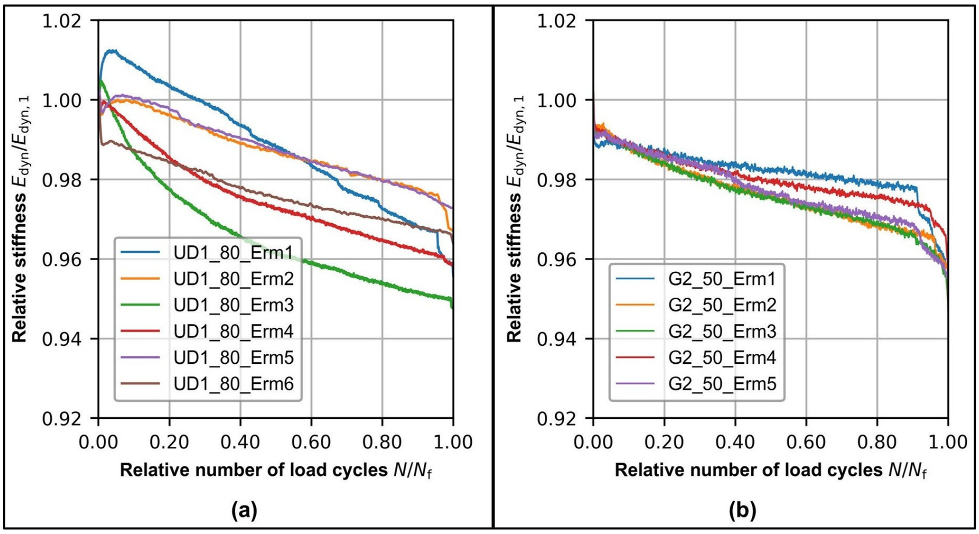

Figure 7. Stiffness degradation during fatigue testing: (**a**) Unidirectional material (80% of UTS^s), (**b**) non-crimp fabric composite (50% of UTS^s). The graphs have been smoothed using a Savitzky–Golay filter (window size of 11 and polynomial order of 1) to reduce noise while preserving the curve shape.

The graphs in Figure 7 show the dynamic stiffness development during fatigue tests on several specimens of the unidirectional material at a stress level of 80% of the UTS^s (Figure 7a) and of the non-crimp fabric laminate at a stress level of 50% of the UTS^s (Figure 7b). They illustrate the individual damage propagation in each test specimen of the fatigue tests, but follow a comparable pattern for both materials in three distinguishable phases. In phase 1, there is a rapid decrease in dynamic stiffness up to approximately 98.8% of the original value. This is followed by an increase in stiffness. For the unidirectional material, this increase typically exceeds the initial stiffness. In phase 2, a continuous decrease in dynamic stiffness is observed. Finally (phase 3), the unidirectional material exhibits a rapid decrease in dynamic stiffness immediately prior to failure, which is not observed for all specimens. This is due to the spalling of some specimens, which was observed during the tests. The non-crimp fabric composite shows a gradual acceleration of stiffness degradation until specimen failure.

3.3. Residual Strength Testing

To evaluate the residual strength behavior of the two materials, the measured residual strengths are plotted against the number of load cycles applied for pre-cycling at 70% of the UTS^s for the unidirectional material and 50% of the UTS^s for the non-crimp fabric composite, respectively (Figure 8).

The residual strengths are shown in Figure 8. Also included are the mean values of the quasi-static tensile strengths of the non-pre-cycled rCF specimens, as well as the standard deviation.

For the unidirectional material (Figure 8a), there is a tendency for the residual strength to decrease compared to the as-manufactured specimens. However, this does not follow a logical trend when considering the various degrees of pre-cycling. This inconsistency is particularly evident in the case of pre-cycling with 3150 load cycles, where the mean residual strength almost reaches the strength of the non-pre-cycled specimens.

When considering the results of the non-crimp fabric composite (Figure 8b), the mean residual strengths show almost no deviation from the strength of the as-manufactured specimens. Only in the case of pre-cycling with 1225 load cycles, a reduction in residual strength is observed. The specimen with the lowest residual strength exhibits an abrupt drop in stiffness shortly before the end of pre-cycling, indicating imminent sudden-death behavior.

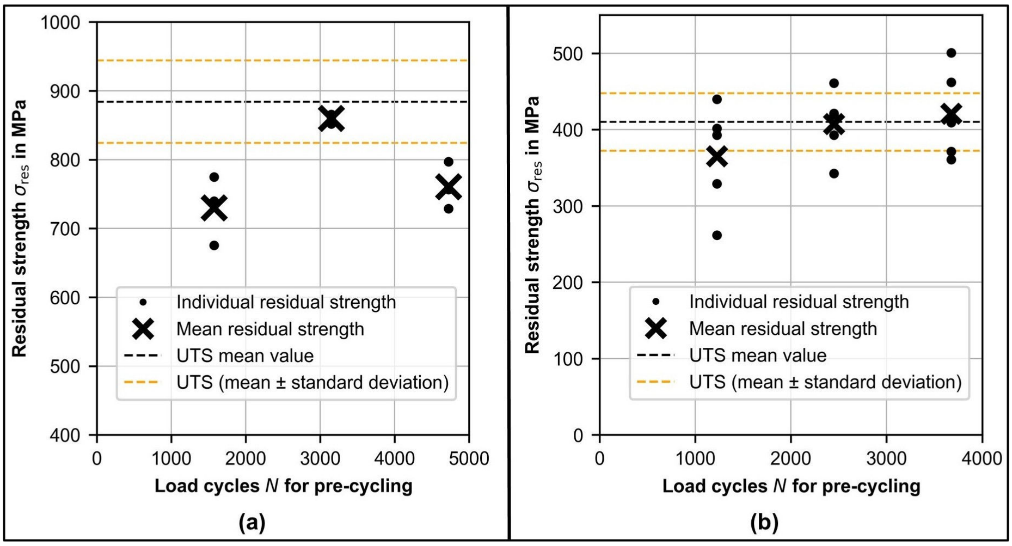

Figure 8. Residual strengths of the materials after pre-cycling: (**a**) Unidirectional material, (**b**) non-crimp fabric composite.

3.4. In Situ Residual Strength Testing

To visualize the in situ residual strength tests, stress-time diagrams are considered (Figure 9). These also include the amplitude of the acoustic activities and the cumulative number of AE hits.

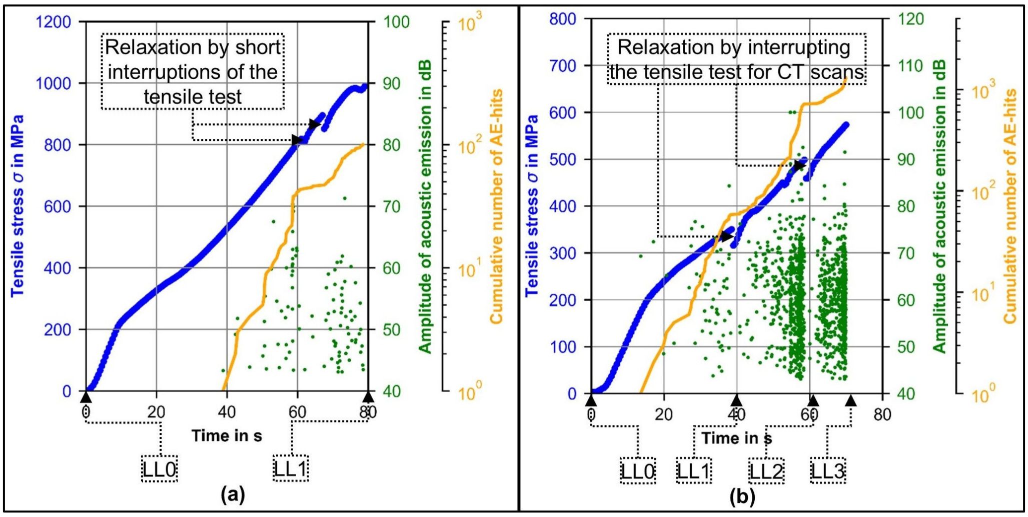

Figure 9. In situ residual strengths of the materials after pre-cycling: (**a**) Unidirectional material, (**b**) non-crimp fabric composite.

The diagrams show relaxations resulting from interruptions in the tensile tests. These interruptions occur either to conduct µCT scans or when approaching the next load level. The times at which the tensile tests were interrupted to conduct a µCT scan are marked in Figure 9 along with the load level. The acoustic hits and their amplitudes are highlighted in green. Before being visualized in the diagram, all hits recorded by the AE system are filtered using a Python (version 3.12) script. The script utilizes the sensor distance and the material's speed of sound to calculate the distance between the acoustic emission source and the sensor based on the arrival times of the acoustic hits at the sensors. This allows filtering so that only the acoustic hits within a radius of 20 mm around the sample center remain (Figure 3a). This section of the specimen includes the narrowest cross-section as well as a part of the transition to the wider cross-section, where damage is suspected to be predominantly located.

To analyze the damage mechanisms during the in situ tensile tests, micro-computed tomography images of the non-crimp fabric composite are shown in Figures 10 and 11, illustrating different damage states at the previously defined load levels.

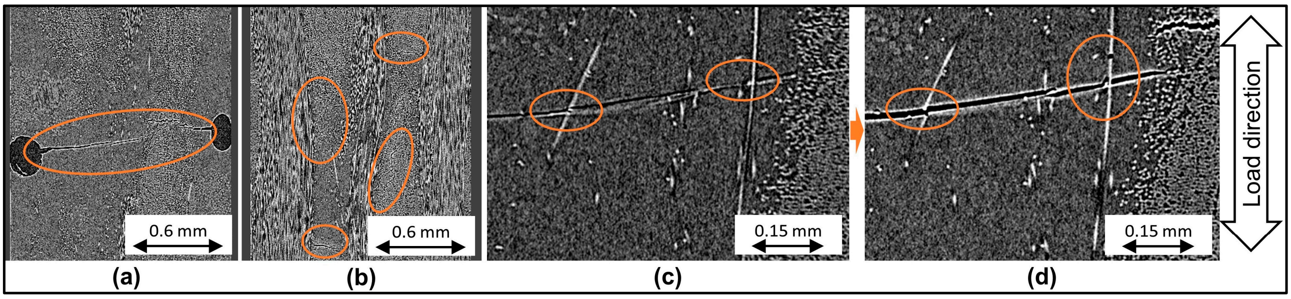

Figure 10. Micro-computed tomography images of the non-crimp fabric composite: (**a**) Matrix crack at near-surface pores at LL0, (**b**) matrix cracks in the 90° layers at LL0, (**c**) fiber-bridged matrix crack at LL0, (**d**) same partly fiber-bridged matrix crack at LL1.

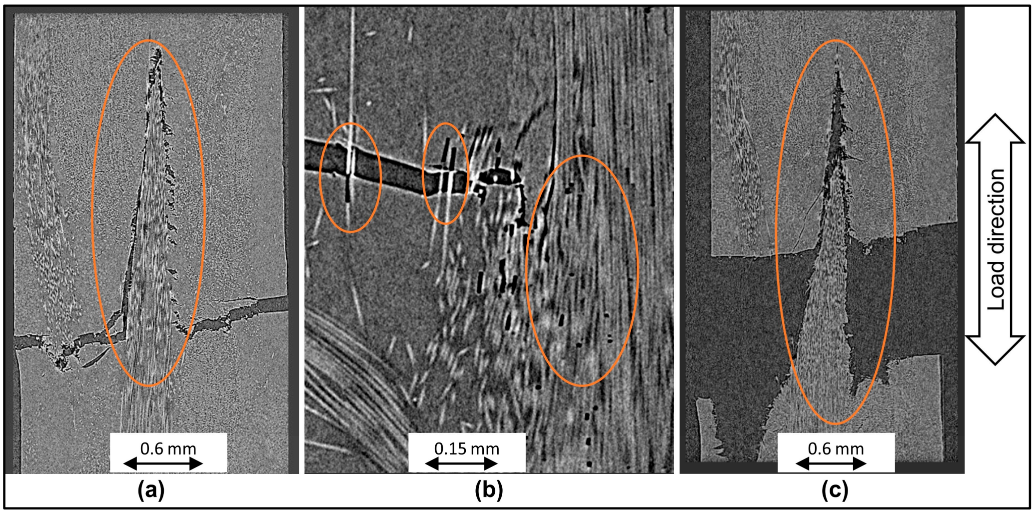

Figure 11. Micro-computed tomography images of the non-crimp fabric composite: (**a**) Crack along layer interface at LL2, (**b**) fiber pullouts and fiber breaks at LL2, (**c**) roving pullout at LL3.

The micro-computed tomography scans of the non-crimp fabric composite show damage in the form of cracks in the 90° layers and resin-rich zones after cyclic pre-damage (Figure 10a,b). At the observed location, a matrix crack initiates at two near-surface pores and propagates perpendicular to the load direction until it reaches adjacent 0° layers (Figure 10a). Additionally, isolated fiber-bridged matrix cracks are observed, which propagate with increasing load level (LL1) and lead to fiber fracture of the bridging fiber (Figure 10c,d).

At load level LL2, a clear progression of damage is seen, characterized by fiber pullout and fiber fractures in the 0° layers, as well as crack propagation at the layer interfaces (Figure 11a,b). This occurs preferably in areas where 90° matrix cracks meet the adjacent 0° layers. Micro-computed tomography observation of the specimen after failure indicates roving pullout as the primary failure mechanism (Figure 11c).

Micro-computed tomography images of the unidirectional material are presented in Figures 12 and 13, illustrating different damage states at the specified load levels during the in situ tensile tests.

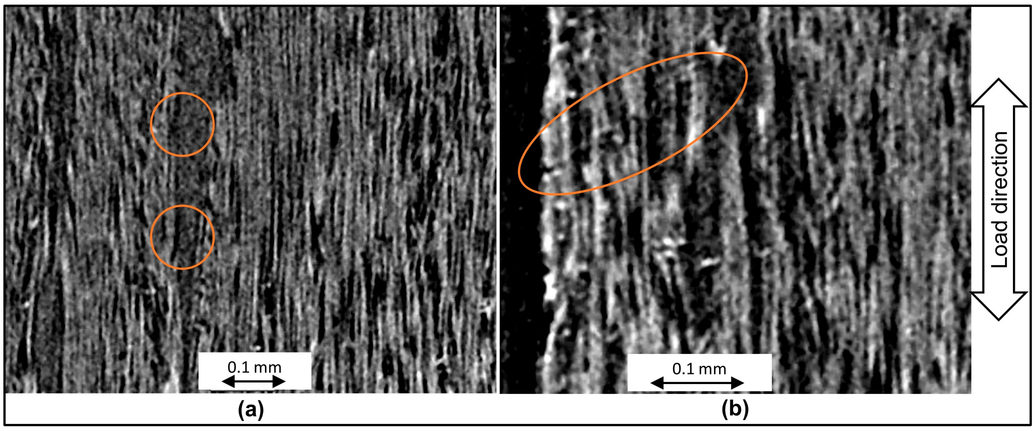

Figure 12. Micro-computed tomography images of the unidirectional material: (**a**) Matrix cracks in resin-rich zones at LL0, (**b**) fiber fractures at the specimen edge at LL0.

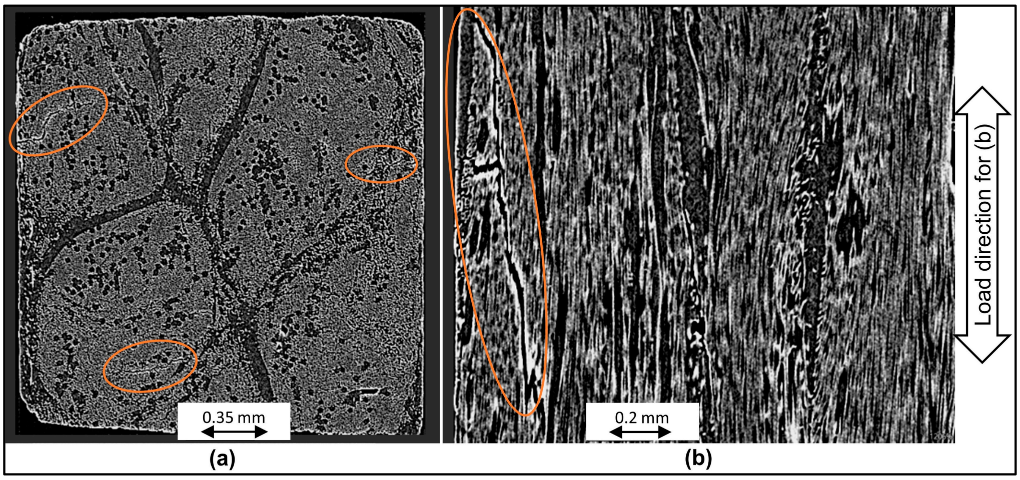

Figure 13. Micro-computed tomography images of the unidirectional material: (**a**) Inter-fiber fractures at LL1 (direction of view in the direction of load), (**b**) inter-fiber and fiber fractures at LL1.

For the unidirectional material, cracks at load level LL0 can be suspected in resin-rich zones due to fatigue loading (Figure 12a). In addition, areas at the specimen edge suggest initial fiber fractures (Figure 12b) due to specimen processing (milling). These areas may favor crack propagation.

After applying load level LL1, clearly identifiable inter-fiber fractures within the rovings and at the roving interfaces (Figure 13a,b), as well as fiber fractures (Figure 13b), can be detected by micro-computed tomography. This corresponds to the typical failure pattern of this material, as already identified from quasi-static tensile testing (Figure 5a).

4. Discussion

The investigation of the quasi-static behavior of the undamaged materials shows that UD1 (FVF of 35%) and UD2 (FVF of 40%) exhibit comparable tensile strengths, which highlights the inhomogeneity of the materials tested. Due to the staple fiber yarn used, the materials contain resin- and fiber-rich areas, as well as other defects (e.g., misaligned fibers) that can influence the tensile strength. When assessing the failure behavior of the UD material and the NCF composite, it becomes clear that the unidirectional material fails due to pronounced inter-fiber fractures in the longitudinal direction of the specimen. In contrast, the non-crimp fabric composite exhibits one or more cracks perpendicular to the load direction.

The comparison of the fatigue properties of the unidirectional rCFRP with the non-recycled continuous fiber reference material [20] is carried out, neglecting the different fiber types and matrices of the two materials. Comparing their fatigue behavior reveals the superiority of the non-recycled fiber composite (vCFRP). The different fiber architectures play a key role, but so do the matrix properties. While the vCFRP consists of continuous fibers, the rCFRP was made from a staple fiber yarn. It can therefore be assumed that the defects in the rCFRP (e.g., resin-rich areas) are significantly more pronounced than those in the vCFRP, which leads to advantages for vCFRP in terms of fatigue properties. The staple fiber yarn may promote the propagation of matrix cracks into the 0° roving near fiber ends of the long fibers, which can lead to crack propagation in the 0° direction (inter-fiber fractures) and reduced fatigue life in comparison to non-recycled continuous fiber composites. Furthermore, yarn undulation leads to excessive stresses due to fiber disorientation. In addition, further inhomogeneities arise due to resin- and fiber-rich areas. Comparing the resin properties of the rCFRP and the reference material, the lower strain at break of the epoxy resin of the rCFRP (5.5–6.5 %) indicates a lower fracture toughness of the matrix, which represents a further advantage of the vCFRP (strain at break (matrix): 7.25% [20]) in fatigue loading. Compared to vCFRP, it can be noted that the rCFRP is primarily affected in the quasi-static regime but less in fatigue loading (Figure 6a). This feature is somewhat unexpected because fatigue loading in the fiber direction is known to cause a high sensitivity toward inhomogeneities like pores and fiber disorientations [9,11].

The behavior of dynamic stiffness degradation in three distinguishable phases can be explained by internal damage development in the materials. The decrease and subsequent increase at the beginning of the test (phase 1) may be a direct result of crack initiation and reorientation processes occurring within the materials. Due to the undulation, the carbon fibers are not perfectly aligned in the load direction, which can result in reorientation under load, leading to an increase in stiffness. The phase of continuous stiffness degradation (phase 2) can be explained by the propagation of damage within the materials. The last section (phase 3) follows because of unstable crack propagation and material spalling immediately before failure. In general, the evolution of stiffness degradation is very close to the well-known behavior of continuous reinforced CFRP [9].

For the residual strength testing, the findings indicate a sudden-death behavior for the UD material and the NCF composite, in which the residual strength decreases only slightly until immediately before failure. Since the residual strength is predominantly influenced by existing material damage, the inhomogeneity of the materials plays an important role. The inhomogeneities of fiber-reinforced plastic composites, and especially of the materials under investigation, result in individual crack initiations and propagations, and thus varying stiffness degradations while pre-cycling. However, the sudden-death behavior is specifically supported by a specimen that exhibits a rapid decrease in dynamic stiffness before the end of the pre-cycling period and a pronounced reduction in residual strength. Due to the inhomogeneities of the materials, the number of specimens tested is critical, which reduces the statistical significance of the investigation. Despite this limitation, a trend can be derived according to which the residual strength behavior is predominantly influenced by local damage and material inhomogeneities.

Comparing the material strengths from the in situ residual strength tests with the standard specimens, increased strengths are observed when testing the tapered specimens, regardless of whether they were previously damaged (Figure 9). This may be a result of the smaller specimen volume and thus a lower probability of defects, or possibly influenced by fiber-rich areas.

Similar to non-recycled fiber composites, the pre-damage in the non-crimp fabric laminate causes cracks in the 90° layers due to the low failure strain of these layers. Existing

https://doi.org/10.3390/jcs10030148

pores also have a crack-initiating effect [9]. When loaded in the residual strength test, crack propagation at the layer interface (delamination) as well as fiber pullout and fiber breakage in the adjacent 0° layers occur. Roving pullout as the primary mechanism before failure can be favored by the crack propagation at the layer interface. It is conceivable that the roving structure (spun long fibers) favors this failure behavior. Matrix cracks in the 90° layers could propagate into the 0° roving structure, which may lead to stepwise crack propagation in the 0° roving.

This can be taken up for the unidirectional material. There, crack initiation can be suspected in areas where fiber breaks can occur due to the statistical fiber strength distribution [9]. Furthermore, the quasi-continuous fiber reinforcement in the rCFRP makes it possible for cracks to initiate at fiber ends, as the fiber end faces are uncoated due to the manufacturing process (i.e., cutting of fibers from production residues) [5]. These areas exhibit reduced fiber–matrix adhesion, which can lead to crack initiation due to the strain concentration between fiber-reinforced regions and resin-rich zones at fiber ends. This was suspected in a study by Klimkeit et al. during fatigue testing of short-fiber-reinforced (30% volume fraction of glass fibers) PBT + PET (polymer mixture) [21].

In addition, areas at the specimen edge that may have been damaged by milling the specimens appear in the form of fiber fractures. After applying an initial load step in the in situ tensile test, pronounced inter-fiber fractures are evident in the 0° direction. These correspond to the typical failure behavior of this material, even when testing standard specimens. The inter-fiber fractures may be the result of transverse contractions or may be caused by matrix cracks that propagate in a stepped manner along the 0° direction. This can be assumed in Figure 13b and leads to the same question as for the non-crimp fabric laminate: How do matrix cracks interact with 0° staple fiber yarns?

5. Conclusions

The experimental investigations in this paper reveal several key findings regarding the mechanical behavior and damage characteristics of two recycled carbon fiber reinforced plastics made from staple fiber yarns. With regard to the unidirectional rCFRP, it is shown that the S/UTS^s-N_f curve exhibits the same slope compared to a vCFRP, despite an overall higher strength of the vCFRP. The stiffness degradations obtained during the fatigue tests show three characteristic phases for the unidirectional material and the non-crimp fabric laminate. However, the failure pattern differs for both rCFRPs, as the UD material predominantly shows longitudinal splitting, whereas the cross-ply NCF layup shows transverse cracking prior to failure. The subsequent residual strength tests show little effect of cyclic loading on the residual strengths of both rCFRPs. In addition, the in situ residual strength tests show that AE is a viable method to determine the onset of damage in in situ µCT experiments. The combination of acoustic emission analysis and micro-computed tomography provides a promising approach for efficiently investigating underlying failure mechanisms in materials at a microscopic scale.

The findings obtained can be used in future studies to specifically optimize the mechanical properties of rCFRP materials made from staple fiber yarns. This can be achieved, for example, by reducing resin-rich zones in the materials to inhibit crack initiation and propagation through improved fiber distribution. It would also be interesting to see how the fatigue properties differ from those of a continuous fiber material when materials with the same fiber type and matrix are compared. Furthermore, as already described above, a detailed analysis of the interaction of matrix cracks with staple fiber yarns would provide further insights into the microstructural behavior of the materials during crack propagation. Finally, the combination of acoustic emission analysis and micro-computed tomography already offers the possibility of an efficient investigation. However, this could be significantly enhanced by an automated link between acoustic emission analysis and control of the micro-computed tomography, as well as the in situ testing device. In addition, the in situ investigation may potentially enable a correlation between acoustic emissions (frequency contents) and the prediction of damage mechanisms.

Author Contributions: Conceptualization, P.R.; methodology, P.R.; software, P.R.; formal analysis, P.R.; investigation, P.R.; writing—original draft preparation, P.R.; writing—review and editing, C.B., A.B., N.M.-E. and J.H.; visualization, P.R.; supervision, N.M.-E. and J.H. All authors have read and agreed to the published version of the manuscript.

Funding: This research received no external funding.

Data Availability Statement: The data that support the findings of this study are available from the corresponding author upon reasonable request.

Acknowledgments: The authors would like to thank Torsten Weick for his assistance in sample preparation. During the preparation of this manuscript, the author used DeepL Write for the purposes of improving the writing style. The authors have reviewed and edited the output and take full responsibility for the content of this publication.

Conflicts of Interest: The authors declare no conflicts of interest.

Abbreviations

The following abbreviations are used in this manuscript:

rCFRP	Recycled carbon fiber reinforced plastic
UD	Unidirectional material
NCF; G	Non-crimp fabric composite
rCF	Recycled carbon fiber
vCFRP	Non-recycled continuous fiber composite
μCT	Micro-computed tomography
LL	Load level
AE	Acoustic emission
FVF	Fiber volume fraction
FRP	Fiber-reinforced plastic

Symbols

The following symbols are used in this manuscript:

F	Force
x	Displacement
L_0	Clamping length
A	Unloaded sample cross-sectional area
s	Standard deviation
S	Maximum stress
N_f	Number of cycles to failure
UTS^s	Ultimate tensile strength at static loading rate
σ	Stress
ε	Strain
E	Young's modulus
ε_m	Strain at break
E_{dyn}	Dynamic stiffness
$E_{dyn,1}$	Dynamic stiffness during the first load cycle
N	Load cycle
σ_{res}	Residual strength

References

1. SGL Carbon SE Batteriegehäuse für Elektroautos. Available online: https://www.sglcarbon.com/loesungen/anwendung/batteriegehaeuse/# (accessed on 26 November 2024).
2. WIN-Verlag GmbH & Co. KG. Airbus A350 XWB Besteht zu 53% aus Kohlefaser-Verbundwerkstoffen. Available online: https://www.plastverarbeiter.de/markt/airbus-a350-xwb-besteht-zu-53-aus-kohlefaser-verbundwerkstoffen.html (accessed on 26 November 2024).
3. VDI Technologiezentrum GmbH. ZRE Wiederverwertung von Carbonfasern aus CFK's. Available online: https://www.ressource-deutschland.de/werkzeuge/ressourceneffizienz-in-der-praxis/innovationsradar/detail/wiederverwertung-von-carbonfasern-aus-cfks/60/ (accessed on 9 December 2025).
4. Pehlken, A.; Albers, H.; Germer, F. Rotorblätter aus Windkraftanlagen—Herausforderungen für das Recycling. In *Recycling und Rohstoffe*; TK Verlag Karl Thomé-Kozmiensky: Neuruppin, Germany, 2017; Volume 10, pp. 247–260, ISBN 978-3-944310-34-3.
5. Hengstermann, M.; Raithel, N.; Abdkader, A.; Hasan, M.M.B.; Cherif, C. Development of new hybrid yarn construction from recycled carbon fibers for high performance composites. Part-I: Basic processing of hybrid carbon fiber/polyamide 6 yarn spinning from virgin carbon fiber staple fibers. *Text. Res. J.* **2016**, *86*, 1307–1317. [CrossRef]
6. Becker, C.; Hausmann, J.; Krummenacker, J.; Motsch-Eichmann, N. First Conclusions on Damage Behaviour of Recycled Carbon Staple Fibre Yarn Using X-ray and Acoustic Emission Techniques. *Materials* **2023**, *16*, 4842. [CrossRef] [PubMed]
7. Detzel, M.; Mitschang, P.; Breuer, U. New Approach for Processing Recycled Carbon Staple Fiber Yarns into Unidirectionally Reinforced Recycled Carbon Staple Fiber Tape. *Polymers* **2023**, *15*, 4575. [CrossRef] [PubMed]
8. Unger, C. Biegen Statt Brechen. *DLR-Magazin* **2020**, *166*, 37–39.
9. Case, S.W.; Reifsnider, K.L. Fatigue of Composite Materials. In *Comprehensive Structural Integrity*; Elsevier: Amsterdam, The Netherlands, 2003; Volume 4, pp. 405–441. [CrossRef]
10. Talreja, R. Fatigue of Composite Materials, Damage Mechanisms and Fatigue Life Diagrams. In *Modern Trends in Composite Laminates Mechanics*; Springer: Vienna, Austria, 2003; pp. 281–294. [CrossRef]
11. Curtis, P.T. Fatigue. In *Mechanical Testing of Advanced Fibre Composites*; Elsevier: Amsterdam, The Netherlands, 2000; pp. 248–268. [CrossRef]
12. Tohgo, K.; Nakagawa, S.; Kageyama, K. Fatigue behavior of CFRP cross-ply laminates under on-axis and off-axis cyclic loading. *Int. J. Fatigue* **2006**, *28*, 1254–1262. [CrossRef]
13. Wagenfelder Spinnereien GmbH Recycling Carbonfaser (rCF) Garne. Available online: https://rcf-yarn.com/de/#garne (accessed on 14 November 2025).
14. *ISO 527-5*; Kunststoffe—Bestimmung der Zugeigenschaften—Teil 5: Prüfbedingungen für Unidirektional Faserverstärkte Kunststoffverbundwerkstoffe. DIN Deutsches Institut für Normung: Berlin, Germany, 2022.
15. *ISO 527-1*; Kunststoffe—Bestimmung der Zugeigenschaften—Teil 1: Allgemeine Grundsätze. DIN Deutsches Institut für Normung: Berlin, Germany, 2019.
16. *ISO 13003*; Fibre-Reinforced Plastics—Determination of Fatigue Properties Under Cyclic Loading Conditions. ISO Internationale Organisation für Normung: Geneva, Switzerland, 2003.
17. *DIN 50100*; Schwingfestigkeitsversuch—Durchführung und Auswertung von Zyklischen Versuchen mit Konstanter Lastamplitude für Metallische Werkstoffproben und Bauteile. DIN Deutsches Institut für Normung: Berlin, Germany, 2022.
18. Vallen Systeme GmbH Acoustic Emission Sensors. 2017. Available online: https://www.vallen.de/wp-content/uploads/2019/03/sov.pdf (accessed on 19 May 2024).
19. Acoustic Emission System AMSY-5 System Description. 2009. Available online: https://www.vallen.de/zdownload/pdf/y5sd0911.pdf (accessed on 20 December 2025).
20. Brunbauer, J.; Pinter, G. Effects of mean stress and fibre volume content on the fatigue-induced damage mechanisms in CFRP. *Int. J. Fatigue* **2015**, *75*, 28–38. [CrossRef]
21. Klimkeit, B.; Castagnet, S.; Nadot, Y.; Habib, A.E.; Benoit, G.; Bergamo, S.; Dumas, C.; Achard, S. Fatigue damage mechanisms in short fiber reinforced PBT+PET GF30. *Mater. Sci. Eng. A* **2011**, *528*, 1577–1588. [CrossRef]

https://doi.org/10.3390/jcs10030148